Water Resources Research

RESEARCH ARTICLE
10.1029/2023WR034790

Large Wood Transport and Accumulation Near the Separation Zone of a Channel Confluence

Saiyu Yuan[1,2], Yuchen Zheng[1], Hongwu Tang[1,2], Yihong Chen[1], Lei Xu[1], Colin Whittaker[3], and Carlo Gualtieri[4]

[1]The National Key Laboratory of Water Disaster Prevention, Hohai University, Nanjing, China, [2]Key Laboratory of Hydrologic-Cycle and Hydrodynamic-System of Ministry of Water Resources, Hohai University, Nanjing, China, [3]Department of Civil and Environmental Engineering, The University of Auckland, Auckland, New Zealand, [4]Department of Structures for Engineering and Architecture, University of Napoli Federico II, Napoli, Italy

Key Points:

- Conducting a laboratory study to investigate the transport, accumulation and trapping mechanism of wood near the confluence
- Evaluating the wood accumulation probability depending on different wood characteristics and confluence hydrodynamic conditions
- Wood released from the tributary may be trapped by the clockwise vortex and thus accumulate in the separation zone

Supporting Information:

Supporting Information may be found in the online version of this article.

Correspondence to:

H. Tang,
hwtang@hhu.edu.cn

Citation:

Yuan, S., Zheng, Y., Tang, H., Chen, Y., Xu, L., Whittaker, C., & Gualtieri, C. (2024). Large wood transport and accumulation near the separation zone of a channel confluence. *Water Resources Research*, *60*, e2023WR034790. https://doi.org/10.1029/2023WR034790

Received 2 MAR 2023
Accepted 12 FEB 2024

Abstract Fallen trees enter the adjacent stream and are carried away downstream by the current. As the stream joins another one, the complex hydrodynamics near their confluence make the movement of wood hard to predict. These woods may accumulate near the confluence resulting in backwater and subsequent potential flooding. A laboratory study was conducted to investigate the movement and accumulation behavior of individual pieces of wood near the confluence. The characteristics of wood (i.e., the length, diameter, and density) and the hydraulic conditions (i.e., the discharge ratio and the release distance) were varied in this investigation. It was found that the wooden pieces released from the tributary got occasionally trapped in the flow separation zone of the confluence, whereupon they were mainly trapped by a clockwise vortex and continued to stay driven by a reverse cluster of currents within this zone. The accumulation probability of wood was mainly related to its length, the discharge ratio and the release distance. The effect of wood diameter and density within the tested parameters was negligible. The probability increased with an increase in the discharge ratio as well as a decrease in the release distance. The longer pieces had a higher probability of being trapped, whereas for those exceeding some critical value, the probability was nearly the same, or dropped sharply. A generalized model for wood accumulation near the confluence was developed for practical application. These findings carry significant implications for river management, particularly in preventing the risk of flooding caused by wood blockage.

1. Introduction

Large wood (LW, e.g. wood floating in a river with a body larger than 1 m in length and 0.1 m in diameter, Keller & Swanson, 1979; Wohl et al., 2010) have received much attention in the past two decades, since they are critical in the river dynamics (Bocchiola et al., 2002; Collins et al., 2002; Gippel et al., 1996; Gurnell et al., 2002; Manners et al., 2007; Schalko et al., 2018; Spreitzer et al., 2021), aquatic ecology (Fausch, 1993; Gurnell et al., 2005; Johnson et al., 2005; Nagayama et al., 2012; Wohl, 2017) and riverine infrastructure (Comiti et al., 2016; Lucía et al., 2015; Ruiz-Villanueva et al., 2014). Trees fall into the adjacent steams due to aging, wind, fire or bank erosion (Benda, Miller, et al., 2003; Lancaster et al., 2003); they are mobilized and transported by the increasing flow depth during flooding, after which they may congregate and even accumulate at bars, islands, floodplains and other river-spanning infrastructures, such as bridges and weirs (Diehl, 1997; Ravazzolo et al., 2022). This may cause backwater flooding and pose potential hazards to riparian areas (Wohl et al., 2016). When the flow conveying the LW joins another stream, the LW transport behavior near the confluence (a critical node in a river system) is unpredictable due to the complex confluence hydrodynamics, and even causes accumulation and jams (Benda, Veldhuisen, & Black, 2003; Benda et al., 2004). Therefore, the present paper investigated the LW transport and potential accumulation near the confluence of two open channels. As a prelude, previous studies related to LW transport and accumulation in a single open channel flow were briefly reviewed. These will provide insight into the basic understanding of the LW movement near the confluence.

Many laboratory and in-situ experiments (e.g., Bocchiola et al., 2006; Braudrick & Grant, 2001; Davidson et al., 2015; Marcus et al., 2002) have been conducted to explore the transport mechanism of LW, which is complex and affected by many factors. For example, 35 core influencing factors were well selected by Wohl et al. (2010), and the study became the cornerstone of later in-stream LW studies. Many studies focused on the transport patterns and travel distance of the floating LW. If the water depth is enough to induce buoyancy, the LW floats and is conveyed by the water flow (Braudrick et al., 1997; Haga et al., 2002). In straight

channels, the pathway followed by LW typically occupies a narrow segment of the channel (Panici, 2021) and aligns with the thalweg (Diehl, 1997), thus facilitating efficient downstream transport (Bocchiola et al., 2006; Braudrick & Grant, 2001). In sharp river bends, it was found that the LW is placed along the thread between the center of the channel and the outside bank (Diehl, 1997), due to helical cells and LW inertia (Innocenti et al., 2023). The distance traveled by LW is related to the LW characteristics (e.g., length, diameter, density and geometry), the channel flow characteristics (e.g., water depth and flow velocity), and in-channel structures. LW pieces with a longer length have a higher momentum, which allows them to overcome frictional resistance, and experienced a wider range of velocities and depths which reduce the influence of local conditions (reductions in depth and velocity) (Innocenti et al., 2023; Ruiz-Villanueva, Wyżga, et al., 2016). The effect of length on travel distance arises from the balance of the two factors, momentum and frictional resistance (Braudrick & Grant, 2001). Welber et al. (2013) found that relative LW diameter strongly reduces wood mobility, with travel distance dropping for diameters exceeding 50% of median channel depth. Likewise, LW with roots were less mobile and therefore less likely to move a long distance (Moulin & Piégay, 2004), the observation by Welber et al. (2013) highlighted that the presence of rootwads affect LW mobility mainly by preventing rolling.

Spanwise or partial LW accumulation near hydraulic structures like bridges and weirs can increase flow resistance, thereby slowing flood flows and raising inundation risks, and cause blockages and damage that escalate flood protection challenges (Comiti et al., 2006, 2016; Lucía et al., 2015; Ruiz-Villanueva et al., 2014; Schalko et al., 2019a, 2019b). Accumulation probability is an important parameter to assess the probability that LW can accumulate near the structures. Previous studies mainly examined the LW accumulation probability near the bridge piers under different conditions, for example, the LW characteristics (i.e., the length, diameter, density, and irregularity of LW, etc.) and flow conditions (i.e., the water depth, flow velocity, Froude number, etc.). Schalko et al. (2020) reported that as LW length increases from 0.1 to 0.4 m, the accumulation probability increases by approximately 40%, demonstrating a significant effect of LW length. A potential reason for this is that the longer wood tends to touch the second pier (where present) during the rotation process after LW touches the first pier. In the approaching river flow, floating LW does not come into contact the riverbed during movement. Therefore, LW diameter and its density seem to have a negligible effect on the accumulation probability (Schalko et al., 2020), as well as the LW geometry (e.g., roots or branches) (Lyn et al., 2003; Schalko et al., 2020). The probability of accumulation for low flow velocities, or low Froude numbers, is generally high (Bocchiola et al., 2008; Haga et al., 2002; Schalko et al., 2020; Schmocker & Hager, 2011). However, the accumulation probability seems to be governed by the flow velocity rather than the Froude number (Lyn et al., 2003; Schalko et al., 2020). LW transported from high velocity may touch the bridge pier but even pass by due to increased turbulence, waves, and vertical flow components (Schalko et al., 2020; Schmocker & Hager, 2011).

Confluences act as critical nodes in river network, characterized by the complex three-dimensional variations in hydrodynamics and bed morphology (Gualtieri et al., 2019, 2020; Tang et al., 2023; Yuan et al., 2019; Yuan, Xu, et al., 2022; Yuan, Zhu, et al., 2022). Six distinct regions characterize flow dynamics at channel confluences: flow stagnation, flow deflection, shear layer, flow separation, maximum velocity, and gradual flow recovery (Best, 1987; Figure 1). The separation zone (e.g., Best & Reid, 1984) and the shear layer (e.g., Rhoads & Sukhodolov, 2004, 2008; Xu et al., 2022; Yuan et al., 2018) are of particular research interest. The separation zone develops when the momentum of incoming flow from an angled tributary has sufficient inertia that it detaches from the channel wall. It lies in the receiving channel near the downstream junction corner. The width and length of the separation zone increase with the discharge ratio and largely affected by the bed morphology (Best & Reid, 1984; Yuan, Yan, et al., 2023). The separation zone is characterized by recirculating fluid and the incoming sediment from the tributary could be trapped by this flow and then deposited therein (Best, 1988; Rhoads, 2020). The shear layer is characterized by increased turbulence levels, with a significant velocity gradient between the two combined flows (Yuan et al., 2018). This enhances turbulent mixing and exchange of momentum and other matter (Rhoads & Sukhodolov, 2001; Yuan et al., 2021; Yuan, Qiu, et al., 2023). This complex confluence hydrodynamics makes the LW movement unpredictable.

The present study presents a series of experiments conducted to investigate LW transport and accumulation at a laboratory-scale confluence, and we assume that the condition is sediment-free, and without regard to the wood-wood interaction and the effects of the wood geometry (roots or branches). The primary objectives of this work were to: (a) investigate the LW motion and characterize the LW trapping mechanism at the confluence and (b)

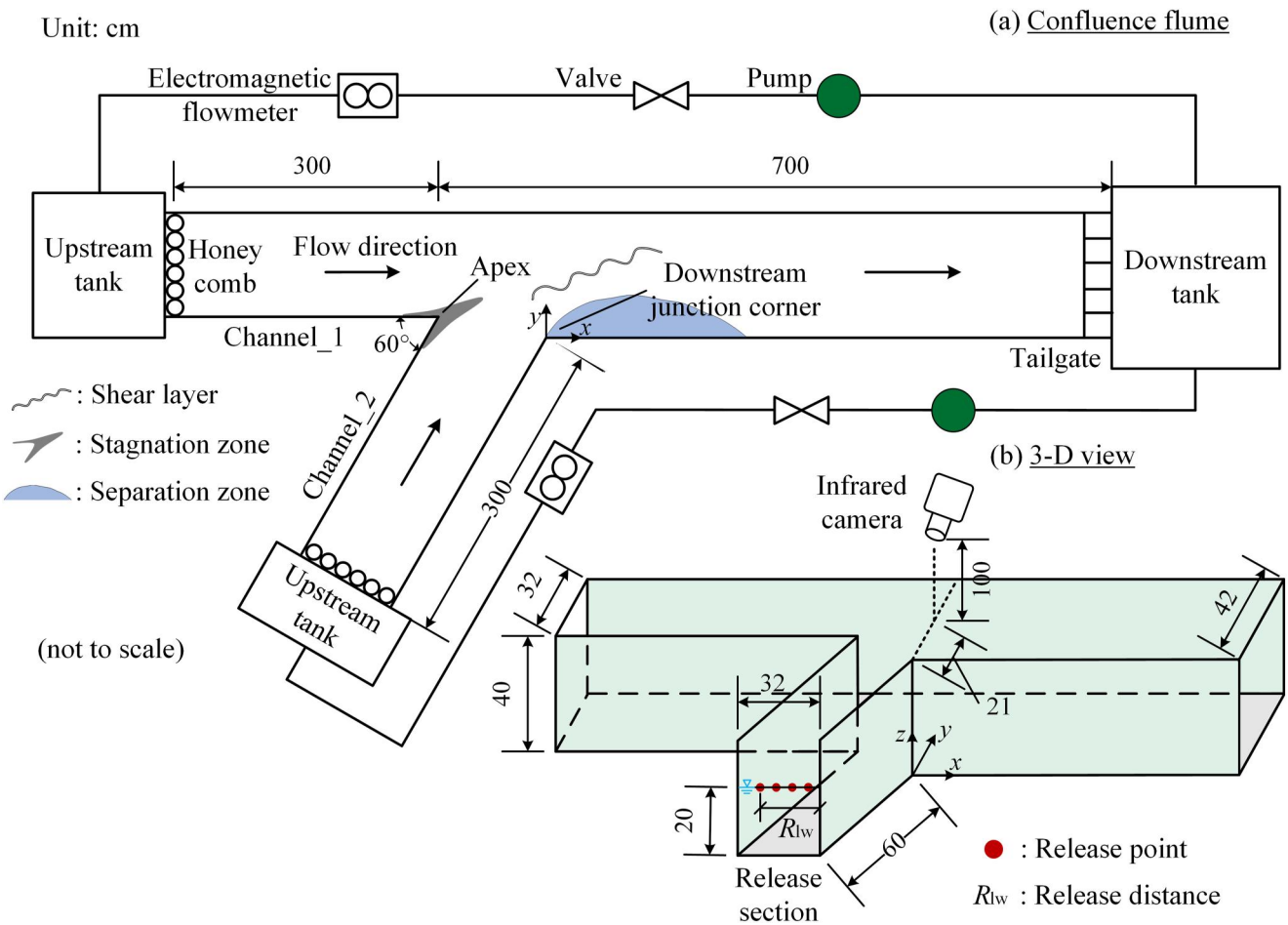

Figure 1. Sketch of the experimental setup including (a) a confluence channel flume with a 60-degree junction angel and (b) a 3-D view of a portion of the flume, including the position of the infrared camera and a detailed arrangement within the release section in Channel_2.

evaluate the potential LW accumulation probability depending on different LW characteristics (wood length, diameter and density) and confluence hydrodynamic conditions.

2. Experimental Setup, Instrumentation, and Data Post-Processing

2.1. Physical Model, Model LW and Measurement

Experiments were carried out in a laboratory-scale confluence assembled at the Laboratory of Sediment of Hohai University, Nanjing (China). The total length of the flume was 10 m. Both the upstream channels, Channel_1 and Channel_2, were 3 m long and 0.32 m wide each, and the length of the post-confluence channel was 7 m, and the width was 0.42 m. The ratio of the width of the post-confluence channel to that of the upstream branches was about 1.3. Such conditions were common in confluent rivers (Yuan et al., 2016). The junction angle was 60°, and all channels had a rectangular cross-section and a flat smooth bottom. Water was pumped from the downstream reservoir to two upstream tanks via 110 mm diameter PVC pipes, and the flow discharge was closely controlled by two ultrasonic flow meters (accuracy ± 0.01 L s^{-1}) and a pump valve system. Honeycombs and sufficiently long straighteners were used to ensure that the flow into the junction was fully developed. The water level was regulated by a downstream tailgate and measured by a ruler against the side wall (accuracy ± 0.1 cm). The laboratory-scale confluence is schematically shown in Figure 1.

An infrared camera (DS-2CD4DP15), fixed at 1 m above the flume confluence, recorded the trajectory of the LW movement with a frame rate of 25 Hz. The trajectory of the LW was post-processed by Logger Pro 3.14.1. By establishing a coordinate system (*x*-*y* plane, as shown in Figure 1), the coordinates of the LW motion process were

Table 1
Hydraulic Experimental Conditions

			h (cm)		Fr (−)			Re (−)		
q_r	Q_1 (L s^{-1})	Q_2 (L s^{-1})	h_1	h_2	Channel_1	Channel_2	Post-confluence	Channel_1	Channel_2	Post-confluence
0.70	6.0	14.0	20.2	20.3	0.07	0.16	0.17	9,537	22,253	24,221
0.61	6.0	9.5	20.2	20.2	0.07	0.11	0.13	9,537	15,100	18,771
0.53	6.0	6.8	20.2	20.2	0.07	0.08	0.11	9,537	10,808	15,501
0.45	6.0	5.0	20.2	20.2	0.07	0.06	0.09	9,537	7,947	13,321
0.35	6.0	3.3	20.2	20.1	0.07	0.04	0.08	9,537	5,245	11,263

Note. q_r is the discharge ratio that equals to $Q_2/(Q_1 + Q_2)$; Q_1 and Q_2 are the discharges in Channel_1 and Channel_2, respectively; h_1 and h_2 are the water depths of Channel_1 and Channel_2, respectively, which are measured 20 cm upstream from the apex; Fr is the Froude number equals to $v/\sqrt{gh}$, where v is the velocity of the channel, g is the gravitational acceleration, and h is the water depth; Re is the Reynolds number equals to vL/ν, where L is the hydraulic radius, and ν is the kinematic viscosity.

recorded at intervals of every 5 frames until the normal direction of the LW was parallel to the flow direction. The velocity field with a moving LW near the free surface (1 cm underwater) was measured using a particle tracking velocimetry (PTV) system (Van den Bremer et al., 2019; Whittaker et al., 2015), including a CMOS camera, a laser, seeding, an image acquisition card, a high-performance computer, and PTV image processing software. The CMOS camera model was JAI SP5000-cxp2, with a resolution of 2,560(H) × 2,048(V) pixels and a maximum frame rate of 254.1 Hz. The high-speed CMOS camera captured the illuminated flow pictures with a 100 Hz frame rate and 120 s sampling time, and the flow was illuminated by a laser light sheet generated by a 7.0 W Nd: YAG laser using a cylindrical lens with a wavelength of 532 nm. The CMOS camera lens is Kowa LM25HC. A dark room was arranged around the flume. The optical axis of the CMOS camera was vertically downwards, perpendicular to the laser plane (i.e., the measurement plane, which is a horizontal plane). The fluid tracers were silver-coated hollow glass spheres having a diameter of 50 μm and the density was 1.04 kg/m^3, the flow field images processing was conducted with Streams v2.06 (Nokes, 2017). One hundred consecutive photographs (the interval between two photos was 0.01 s) which captured the trajectory of the LW were selected and the instantaneous flow velocity was calculated using Streams v2.06.

The experiments were conducted under steady flow and sediment-free condition. The hydraulics of LW flow are characterized by the discharge ratio q_r (defined as the discharge of the Channel_2 to the total one). During the experiments, the Channel_1 flow discharge (Q_1) was held constant, and the Channel_2 flow discharge (Q_2) was modified to regulate the discharge ratio. The water stage z was set to 20 cm at 0.5 m upstream of the tailgate, the water depth of Channel_1 and Channel_2 (measured at 20 cm upstream from the apex) are provided in Table 1. The flow discharge, flow velocity, Froude number, and Reynolds number used in the experiments are also shown in Table 1.

Natural woods with constant cylindrical geometry were chosen to represent LW in the experiments, geometrical irregularities (including any rootwads and branches) were excluded to simplify the piece. By referring to two specific ranges of wood density found in previous research: (a) instream wood (a mean value of 660 ± 200 kg/m^3, Ruiz-Villanueva, Piégay, et al., 2016) and (b) waterlogged large wood (with a range of 880–900 kg/m^3, Buxton, 2010), three tree species, namely Betula platyphylla, Styphnolobium japonicum, and Zelkova serrata were used to achieve various densities. Before the experiments, all LW pieces were repeatedly immersed in water to determine their wet density. The LW pieces were considered ready for experimentation once their weight stabilized at a constant value (Innocenti et al., 2023). The average wet density of these models was calculated before the experiment. Henceforth, when referring to LW density (ρ_{lw}), we considered the mean wet density. 3 different average densities (ρ_{lw}, were 680, 800, and 900 kg/m^3 with accuracy ± 50 kg/m^3), 11 lengths (L_{lw}, ranging from 10 to 20 cm with a step of 1 cm), and 3 diameters (D_{lw}, were 0.8, 1.5, and 2.0 cm) with a total 99 length/diameter/density combinations were used. The characteristics of the LW in the experiments are listed in Table 2. The experiment involved the preparation of 15 identical LW pieces for each required combination and each piece was only used twice within a specific condition. The ratio of LW length to the channel width and the LW slenderness are like the ones used in previous field (Abbe & Montgomery, 2003) and laboratory studies (Bocchiola

Table 2
Experimental Series to Study the LW Accumulation Probability

Test series	Tested parameters	q_r, −	ρ_{lw}/ρ_w, −	D_{lw}/h, −	L_{lw}/w_a, −	R_{lw}/w_a, −
A1-A55	L_{lw}, q_r	**0.70, 0.61, 0.53, 0.45, 0.35**	0.90	0.075	**0.238–0.476 (0.024 step)**	0.06
A56-A64	L_{lw}, D_{lw}	0.70	0.90	**0.04, 0.075, 0.1**	**0.238–0.476 (0.119 step)**	0.06
A65-A80	L_{lw}, R_{lw}	0.70	0.90	0.075	**0.238, 0.286, 0.357, 0.429**	**0.06–0.417 (0.119 step)**
A81-A89	q_r, ρ_{lw}	**0.70, 0.61, 0.45**	**0.68, 0.80, 0.90**	0.075	0.357	0.06
A90-A101	q_r, R_{lw}	**0.70, 0.61, 0.45**	0.90	0.075	0.357	**0.06–0.417 (0.119 step)**

Note. Changing parameters are marked in bold, test series A involves the release of LW from Channel_2. ρ_{lw}/ρ_w is ratio of the LW density to the water density (considering $\rho_w = 1{,}000$ kg/m^3); D_{lw}/h is ratio of the LW diameter to the water depth; L_{lw}/w_a is the ratio of the LW length to the post-confluence channel; R_{lw}/w_a is the ratio of the release distance to the width of the post-confluence channel, and the release distance is defined as the distance of the release point from the right bank of Channel_2, the release point is shown in Figure 1.

et al., 2008; Furlan et al., 2021; Schalko et al., 2020; Schmocker & Hager, 2011). In all the experiments, the LW piece was never soaked, and it always floated on the water surface.

2.2. Experimental Procedures

It was found in pre-tests that the LW released in Channel_1 did not stay at the confluence and move downstream, while that released in Channel_2 may accumulate in the separation zone of the confluence. Thus, formal experiment was carried out by adding a single LW into the Channel_2 to the approach flow 60 cm upstream from the confluence apex. The distance ensured that the LW had the same velocity as the free surface when it arrived at the confluence. Each LW was carefully released into the channel by the operator, avoiding interference of the LW and ensuring its initial orientation was parallel to the local flow direction. The LW was released within the release section when conducting test series A1-A101, and the specific release arrangement under different the release distance R_{lw} (defined as the distance of the release point from the right bank of Channel_2) is shown in Figure 1. After each trial, the LW was removed from the flume before the next trial, irrespective of whether the LW accumulated in the separation zone or not. Each test was repeated for 30 times to obtain an estimation error of less than 0.09 (with a confidence level of 90%), the specific selection method is outlined in Section 2.3. Table 2 shows the details of the test series conducted in Channel_2.

Five dimensionless quantities were introduced here. They are: (a) the ratio of the wood length to the post-confluence channel width (L_{lw}/w_a), (b) the ratio of the wood diameter to the water depth (D_{lw}/h), (c) the ratio of the wood density to the water density (ρ_{lw}/ρ_w), (d) the ratio of the release distance to the post-confluence channel width (R_{lw}/w_a), (e) the discharge ratio (q_r).

2.3. Statistical Analysis and Test Repetition

Accumulation of LW means that LW is trapped in the separation zone and remains attached to the right bank. Consequently, the accumulation probability (AP) is defined as the ratio of the accumulated LW in a specific configuration to the number of repetitions. The accumulation probability of LW was estimated using the experimental results. Each trial was considered a Bernoulli trial where only two outcomes were possible: either the LW was transported downstream resulting in an accumulation probability $AP = 0$, or it was trapped in the separation zone yielding an accumulation probability $AP = 1$ (Furlan et al., 2019; Schmocker & Hager, 2011). The accumulation probability of LW in each test was denoted by AP and 1-AP the probability of passage. The maximum likelihood estimator $\widehat{AP}$ was used to estimate the accumulation probability, AP:

$$\widehat{AP} = \frac{m}{n} \tag{1}$$

Where n is the number of repetitions in each test, and m is the number of trapped LW, and confidence intervals with 90% confidence was calculated based on the Wald method, as given in Furlan et al. (2019).

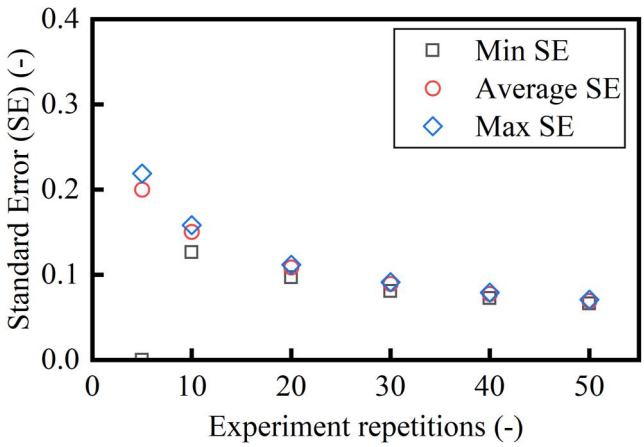

Figure 2. Maximum, minimum, and average standard error values for different experimental repetitions with the 300-repetition test.

To obtain statistically significant results for accumulation probability, the number of repeated experiments n should be determined. Furlan et al. (2020) suggested that the number of repetitions should be at least 30 times to obtain an estimation error of less than $max\ SE = 0.09$ ($max\ SE = \sqrt{\frac{0.5(1-0.5)}{n}}$), with a confidence level of 90%. In the present study, an initial 300 repetition test was conducted (with a run of $L_{lw} = 15$ cm, $D_{lw} = 1.5$ cm, $\rho_{lw} = 900$ kg/m^3 and $q_r = 0.70$, $R_{lw} = 2.5$ cm) to calculate the standard error for the number of experiment repetitions ranging from 10 to 50, step by step (in steps of 10). For example, when the number of experiment repetitions is 10, the standard error is calculated first based on the results of 1–10 experiments. This is followed by calculations making use of the results of 2–11 experiments, and repeating others in this manner. After calculating the standard errors of all groups, the maximum, minimum, and mean values of standard errors were found, respectively (Figure 2). As the maximum value of the standard error was lower than 0.1 for 30 repetitions, it was considered as reasonable to conduct 30 repetitions for each test.

3. Results

The following sections explore the flow patterns of LW near the confluence, estimate the LW accumulation probability by considering several characteristics of the LW (i.e., the length L_{lw}, diameter D_{lw}, and density ρ_{lw}) as well as flow conditions (i.e., discharge ratio q_r and release distance R_{lw}). Subsequently, the analysis is further extended to the LW transport mechanism by investigating the velocity field near the free-surface.

3.1. LW Motion Patterns

In the test series A, the LW released from Channel_2 could occasionally be trapped into the flow separation zone and subsequently accumulate in this zone. Figure 3 visualizes the main distinct transport patterns, including the trapping one, escaping one and '*margin-impact*' mode. Figure 3a shows the trapping processes, which mainly included: the LW being conveyed along the boundary of the flow separation zone (I), and subsequently revolving clockwise (top view) (II), until its long axis was perpendicular to the x-direction (III), and moving in the reverse direction (i.e., -x direction). Finally, it attached to the right bank and accumulated in the flow separation zone (IV). LW that were not trapped by the separation zone may also undergo revolving during the escaping processes (Figure 3b). However, they continued to move downstream in the direction of the flow eventually.

Moreover, longer pieces of LW had the potential for touching the flume sidewall during their motion, which is referred to as the '*margin-impact*' mode (Figure 3c). Two subsequent major patterns of LW motion were observed: (a) the LW rotated anti-clockwise and mostly settled in the separation zone while a small portion of the LW still moved downstream due to the randomness, and (b) the LW rotated clockwise then moved downstream after the contact. These two patterns were related to the LW motion when and how (particularly the impact angle) it touched the channel wall, as well as the instantaneous water flow around the LW. As it was a complex and random process, it was difficult to predict the subsequent motion of the floating wood.

3.2. Effect of LW Length and Discharge Ratio on LW Accumulation Probability

Figure 4a presents the variation of the accumulation probability (AP) with L_{lw} under different q_r. For the cases with smaller q_r (i.e., $q_r = 0.35$ and 0.45), AP linearly increased as a function of the LW length ($R^2 = 0.92$). The probability peaked when the LW length reached some critical value, and further increase in L_{lw} caused a rapid decrease of the AP, even plummeting to zero. The maximum change in AP due to L_{lw} variation was around 40% under the smaller q_r. With the increase in q_r, the AP increased correspondingly. Smaller AP for the $q_r = 0.53$ than that for the larger q_r was observed before attaining the peak, though the difference was not significant (~6%). The highest AP value was around 0.5 for L_{lw}/w_a about 0.33 (i.e., $L_{lw} = 14$ cm with a test range of 10–20 cm), which was approximately 20% higher than that for the shortest LW. After AP peaking, there exists a relatively stable state (defined as a range where the difference is less than 10%) for the higher q_r, and this stable state could keep longer as the q_r increase. Particularly for the cases with $q_r = 0.70$ and 0.61, when the L_{lw}/w_a larger than 0.33, the

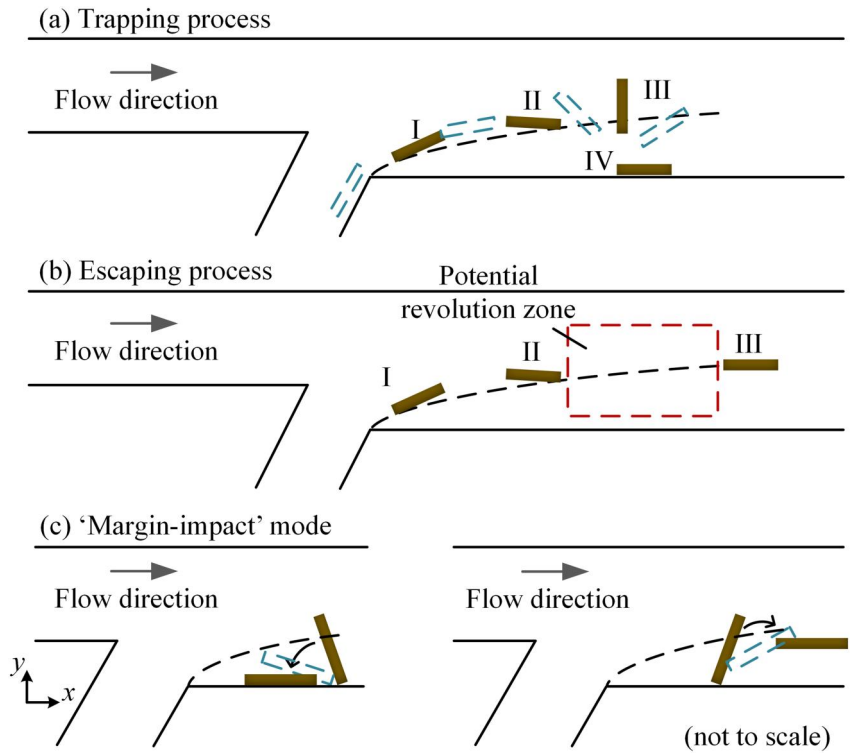

Figure 3. The sketch of LW trajectory near the separation zone includes: (a) the main trapping process with four phases (I) the LW was advected to the upstream of the separation zone (II) and then revolved along the boundary of the separation zone ending at a specific position (a rotation was considered as complete when the LW long axis was perpendicular to the flow direction in the *x*-direction) (III) the revolved LW entered and accumulated in the separation zone (IV) and finally attached to the right bank, (b) the escaping process, (c) the '*margin-impact* mode'. The green dashed rectangular box is the transition state, the red dashed rectangular box is the potential revolution zone, the black dashed line is the boundary of the separation zone.

APs were all about 0.45 with a deviation of less than 5%. Such deviation is even within the allowable range of repeatability (10%).

3.3. Effect of LW Diameter and Density on LW Accumulation Probability

The effect of wood diameter D_{lw} on *AP* was investigated by testing three different diameters with various L_{lw} (Figure 4b). For all tests having the same L_{lw}, the deviation of *AP* for various D_{lw}/h was within 10%, which is in

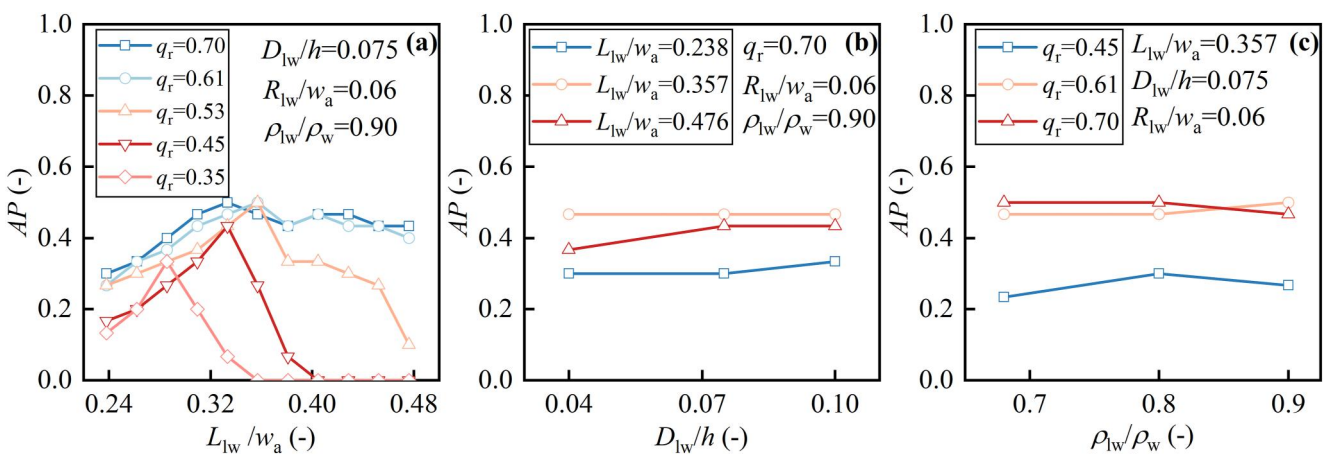

Figure 4. Accumulation probability (*AP*) versus (a) LW length L_{lw} and various discharge ratio q_r with test series A1-A55, (b) LW diameter D_{lw} and various LW length L_{lw} with test series A56-A64, (c) LW density ρ_{lw} and various discharge ratio q_r with test series A65-A80.

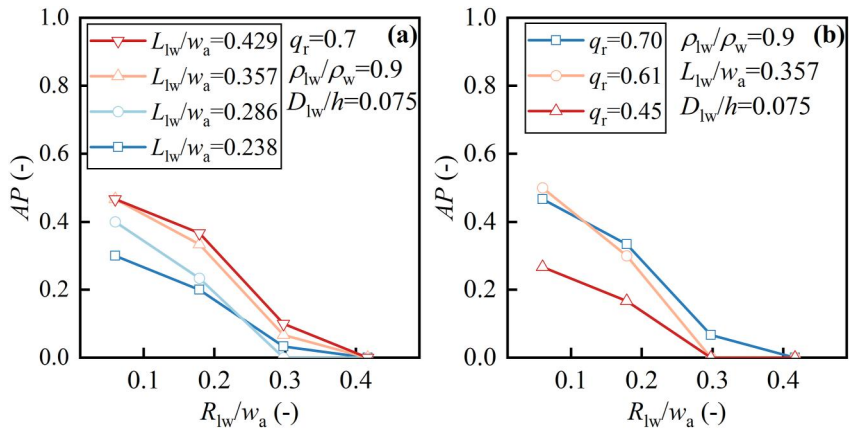

Figure 5. Accumulation probability (*AP*) versus (a) release distance R_{lw} and various LW length L_{lw} with test series A81-A89, (b) release distance R_{lw} and various discharge ratio q_r with test series A90-A101.

the allowable limits for reproducibility. Thus, the effects of D_{lw} on *AP* were minor compared to the L_{lw}. Figure 4c shows the effects of LW density ρ_{lw} on *AP*. It was found that the variation in ρ_{lw}/ρ_w did not affect the *AP* significantly. Although some deviation in *AP* was observed, it was within the range allowed by reproducibility.

3.4. Effects of Release Distance on LW Accumulation Probability

In Figure 5, the *AP* of LW is plotted versus the release distance R_{lw}/w_a. A clear trend can be seen from the graph that the *AP* significantly decreased with the increase of the release distance, as the R_{lw} increased the *AP* decreased until approaching zero. The *AP* deviation corresponding to $R_{lw} = 2.5$ cm and $R_{lw} = 17.5$ cm for $L_{lw} = 15$ cm could reach 50%. When R_{lw} exceeded 12.5 cm, LW could hardly accumulate in the separation zone. Figure 5 also shows the relationship between the R_{lw} and *AP* under different L_{lw} and q_r, with a noticeable similar trend. As the q_r and L_{lw} decreased, the R_{lw} needed to prevent wood from being trapped in the separation zone decreased accordingly.

3.5. Dynamic Response of LW to Free-Surface Flow

In this section the LW trapping mechanism is explored by investigating the velocity field near the free-surface (the plane 1 cm under the surface) under two different q_r. It was observed that two main vortices V1 and V2 lay within the separation zone and a reverse current was found longitudinally regardless of q_r, and the scale of these vortices was positively correlated to the q_r (Figure 6). The variation in the scale of the V1 vortex was particularly evident, with the width of the vortex reaching approximately 10 cm (i.e., about 0.25 w_a) as the q_r reached to 0.70 from 0.45. Figure 6 also shows the LW transport process along with the distribution in the plane *xy* of velocity vectors (*u*, *v*). The trajectory of the LW always followed the boundary of V1 vortex and entered the separation zone at the downstream boundary of V1. Meanwhile, LW was perpendicular to the *x*-direction.

Figure 7 shows the box plot of the LW rotation end position (i.e., when the LW long axis is first perpendicular to the *x*-direction as the time when the wood element enters the separation zone) for test series A1-A11 (i.e., $L_{lw} = 10$–20 cm, $D_{lw} = 1.5$ cm, $\rho_{lw} = 900$ kg/m^3 and $q_r = 0.70$, $R_{lw} = 2.5$ cm). The end position ranged from 20 to 45 cm, and the average was around 33 cm. The accumulation pattern for all the tested LW pieces (regardless of different characteristics) was similar, as discussed in Section 3.1. Hence, it can be inferred that the primary driver of LW accumulation in the separation zone was V1 vortex. Therefore, the fluctuation of the V1 vortex resulted in slight variations in the end position of the LW. Although the downstream boundary of the V1 vortex was relatively stable (around 33 cm) under a large sample statistic, some variations may be due to the random evolution of the V1 vortex and the complex interaction between the wood and the V1 vortex.

4. Discussion

4.1. Analysis of LW Transport Near the Separation Zone

This section aims to analyses the LW transport along the boundary of the separation zone. First, we assume that the lift force (as shown in Figure 8, denoted as F_l) acting on the LW dominates the movement, and this force is

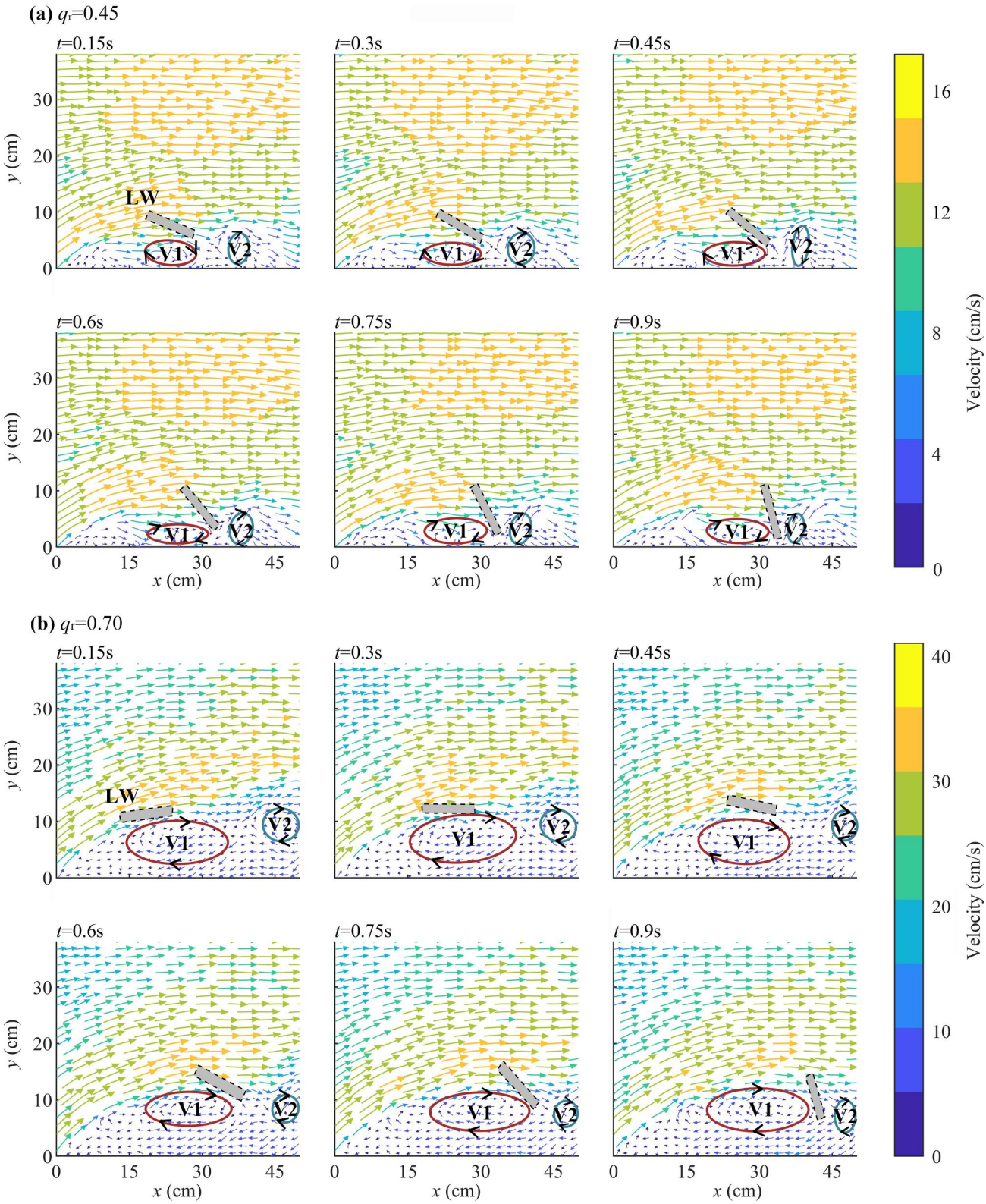

Figure 6.

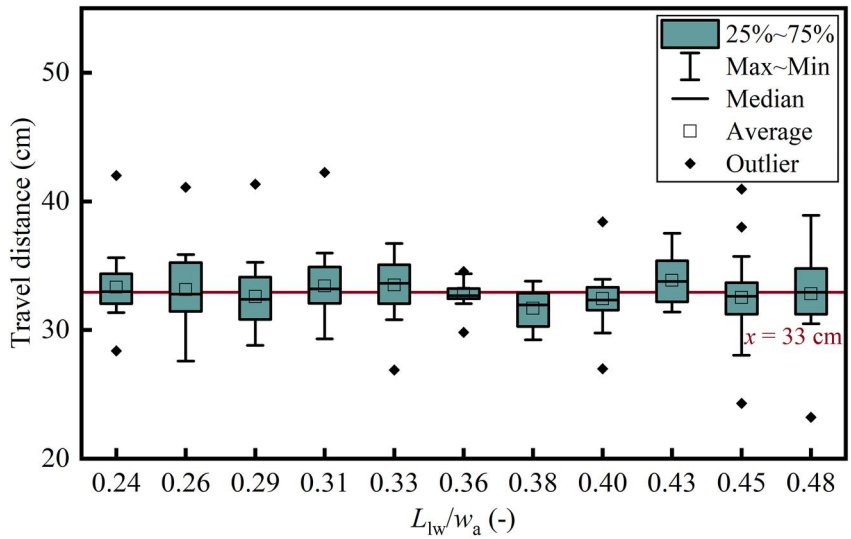

Figure 7. Box plot of the LW travel distance, the data are derived from test series A1-A11. The red line ($x = 33$ cm) represents the average of all travel distances.

perpendicular to the LW. Second, the vortex size in the separation zone is large enough so that LW could rotate driven by the vortex, and the vortex driving the LW rotation was assumed as a circular with the diameter D_s (unfortunately not quantified in this study). Last, the LW can follow a circular pathway under the action of lift force and subsequently accumulate in the separation zone (Figure 8). Therefore, the velocity (v_c) when LW is moving with a circular motion could be estimated according to the centripetal force equation (simplifying the LW as a point mass situated at the center of mass of the wood):

$$v_c = \sqrt{\frac{F_l D_s}{2m}} \tag{2}$$

where the F_l is the lift force, D_s is the vortex diameter, and m is the mass of the wood. We can consider that when the velocity of LW is less than or equal to v_c, the LW would be captured into the separation zone by the vortex. On the other hand, if the velocity of LW is too large, it can escape from the effects of the vortex and move downstream. At this point, we have developed a hypothesis model that examines whether wood accumulation within the separation zone is determined by the relative magnitudes of the v_c (associated with the centripetal force acting on the wood) and the velocity of the wood itself. The speed of the wood is affected by the complex interaction between wood and flow, which is hard to be estimated. v_c changes as the average pressure associated with the instantaneous flow velocity and the angle between the wood and the flow direction changes randomly. The *centripetal force* itself is related to the scale and the intensity of the vortex (i.e., the tributary discharge) and the length of wood. Besides, the distance between the wood and the core of the vortex could also affect their interaction, and this distance is not constant even under the same experimental condition. Nonetheless, Equation 2 could qualitatively explain the influence of various factors on the transport and accumulation of wood near the separation zone. It will be elaborated upon later.

4.2. Generalized Statistical Model of LW Accumulation Probability

As shown in Section 3.1, the motion pattern changed when the length of the wood exceed some critical value, which may be related to the excess size of the wood larger than the vortex size and/or the more frequent

Figure 6. Velocity field near the free-surface (1 cm underwater) of LW accumulation process in the separation zone with the corresponding schematic position of LW including (a) the accumulation process of LW with a run of $L_{lw} = 12$ cm, $D_{lw} = 1.5$ cm, $\rho_{lw} = 900$ kg/m^3 and $q_r = 0.45$, $R_{lw} = 2.5$ cm and (b) the accumulation process of LW with a run of $L_{lw} = 10$ cm, $D_{lw} = 1.5$ cm, $\rho_{lw} = 900$ kg/m^3 and $q_r = 0.70$, $R_{lw} = 2.5$ cm. The red ellipse represents vortex V1, the green ellipse represents vortex V2. The multicolored background arrows indicate the velocity vector of the near free-surface, and the arrow size represents the local flow velocity magnitude (the corresponding color in the colorbar can also indicate the velocity magnitude).

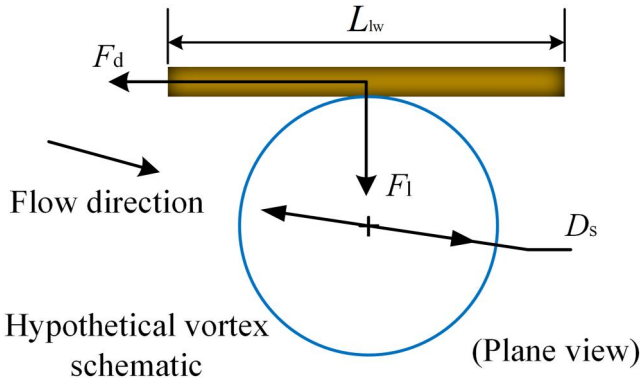

Figure 8. The schematic diagram representation of LW and the vortex, the brown rectangle represents LW, and the blue circle represents the hypothetical vortex, L_{lw} is the length of the LW, D_s is the width of the separation zone. F_l and the F_d are the lift force and the drag force acting on the LW, respectively.

occurrence of the *margin-impact* mode. In this study, only the data pertaining to the increasing *AP* phase (i.e., the shorter wood than the critical value) were used (eliminating duplicates) to derive the statistical model. The data set used in this generalized statistical model is provided in the Supplementary Material S1.

The following equation was developed based on nonlinear regression analysis to quantify the accumulation probability:

$$AP = 0.18\left(\frac{L_{lw}}{w_a}\right)^{1.68}\left(\frac{R_{lw}}{w_a}\right)^{-1.12} q_r^{\,0.69}\,(L_{lw} \le L_{lw,c}) \quad (3)$$

where $L_{lw,c}$ is the critical value of the wood length when the accumulation probability peaks. $L_{lw,c}$ is related to the size of the vortex/the separation zone. The negative sign of the estimated exponent for R_{lw}/w_a indicates that a decrease in the release distance increases the accumulation probability. The positive sign of the estimated exponents for L_{lw}/w_a and q_r indicates that the increase of the wood length or the discharge ratio results in increase of the accumulation probability. The increase in the q_r resulted in a higher hydrodynamic pressure on LW, thus promoting downstream transport. However, a larger q_r also led to a larger separation zone and more intensified vortices, thereby facilitating the trapping of LW by the V1 vortex and its subsequent accumulation. Based on the experimental results and the preceding analysis, it can be inferred that the latter aspect plays a more important role in LW transport, which accounts for the positive exponent of q_r. The regression analysis is provided in the Supplementary Material S1. As with any empirical formula, application of Equation 3 is limited to the range of tested parameters.

4.3. Effects of the Studied Variables on the Accumulation Probability

In the present study, the LW accumulation probability in the separation zone can only be determined experimentally while the proposed conceptual model (Section 4.1) provides a basis to characterize the transport mechanism of LW to free-surface flow near the separation zone. The effect of each parameter on the LW accumulation process near the separation zone is discussed below.

Before *AP* peaking, an increase in L_{lw} resulted in a larger *AP* near the separation zone (Figure 4). It was followed by a dip. Longer LW integrated a wider range of water velocities which was more likely to be affected by surface flow turbulence. Rotation was further promoted for the larger LW compared to the shorter ones. This is corresponding to the rising phase in Figure 4a. However, longer wood also has a greater inertia, with a less likely rotation and accumulation in the separation zone. These two mechanisms apply to wood of any length; it's just that under higher q_r, the scale and intensity of the vortex are relatively larger, providing a higher level of tolerance for the competition between these two mechanisms. The competition between these two mechanisms persists until the scale of the LW (mostly related to LW length) was much larger than the scale of the vortex. When the scale of the LW exceeded the scale of the vortex, the LW was less likely to rotate in response to the vortex, resulting in a lower *AP* eventually. This can explain why there is a relative long stable step in the accumulation probability under high confluence ratios. Under lower q_r we infer that there should also exist a stabilization phase, albeit shorter than the higher q_r one. This different phenomenon may be related to the limitation of wood size increasing steps and separation zone size in experimental conditions. The other factor affecting the accumulation probability was the *margin-impact* mode as discussed in Section 3.1, this mode was observed if the LW was larger than the vortex. It is expected that the *margin-impact* mode to exert first-order control on the rotational LW motion as the L_{lw} gradually increases and/or as the q_r gradually decreases. This aspect was not investigated in the present study due to the limitations of the flume and wood. The effect of L_{lw} on *AP* was different from the previous observations conducted in an open channel flow due to the more important wood-flow interaction. In an open channel, longer LW had a higher *AP* simply because their length spanned major parts of the channel or were more likely to be pushed out of the thalweg and encounter high friction zones (shallow regions) with subsequent accumulation (Braudrick & Grant, 2001).

The present results on the effect of D_{lw} and ρ_{lw} on AP agreed with previous studies related to LW motion. Once the LW was fully floating, the effect of D_{lw} and ρ_{lw} on accumulation was minor. Schalko et al. (2020) investigated the effect of ρ_{lw} on the AP at bridge piers and found that when ρ_l was below 1,000 kg/m^3, the LW was fully floating, suggesting a negligible effect. Additionally, the tested wood exhibited the different D_{lw} and the similar ρ_{lw} but were transported in a comparable pattern, which may explain why D_{lw} did not significantly affect AP. However, the impact of D_{lw} and ρ_{lw} might be important if LW reaches the channel bed or touches any in-stream structure.

In addition, the approach flow conditions, that is, q_r, were expected to play an important role in the AP at the confluence. A higher q_r led to an increase in the size of the separation zone. According to Equation 2, the critical velocity v_c increased and this in turn enhanced inclusion of LW with higher velocity. Furthermore, an increase in q_r increased the geometric scale of the vortex in the separation zone and hence the AP. It is important to note that the aforementioned relationship holds true only within a specific range of R_{lw}. The R_{lw} was driving the initial position of the wood at the confluence and its subsequent trajectory. An increase in R_{lw} results in the wood being positioned further away from the boundary of the separation zone. Consequently, the likelihood of interaction between the wood and the vortex structure within the separation zone diminishes, leading to a lower AP. Moreover, if the LW was conveyed by the mainstream (Channel_1 in this study), the shear layer formed at the convergence of the two incoming surface flows acts as a barrier, impeding the wood from moving toward the separation zone (Yuan et al., 2018; Yuan, Yan, et al., 2023).

In natural channels, the banks of the post-confluence channel might have plants and vegetation, which could affect the *margin-impact* pattern. In addition, LW transport in rivers often occurs in a continuous way, with a complex wood-wood interaction in addition to the wood-flow interaction. Moreover, natural wood often has rootwads, branches and so on, and the dynamic response of these complex LW structures to flow might be different. Numerical modeling of the complex wood-wood interaction (Persi et al., 2018, 2019) is valuable to investigate the wood transport near the confluence, including the contribution of the hydrodynamics parameter.

5. Conclusions and Outlook

Flume experiments were conducted to investigate the transport and accumulation of large wood at a laboratory-scale confluence. The objective was to investigate and clarify the interaction between the wood and the free-surface flow under conditions without sediment and discarding wood-wood interaction. The key findings of this study are the following.

1. The wood released from Channel_2 accumulated in the separation zone at the right bank of the confluence with a probability ranging from 0% to 50%, while that released from Channel_1 did not accumulate therein.
2. The behavior of the wood trapped in the separation zone was well captured. During the trapping the wood was conveyed along the boundary of this zone, rotated clockwise subsequently, moved in the upstream direction and finally attached to the right bank and stayed in the separation zone. Longer woods (compared with the scale of the vortex in the separation zone) touched the channel bank and those anti-clockwise rotating settled in the zone, while those clockwise rotating moved downstream.
3. By PTV measurement, it was found that wood was mainly trapped in the separation zone by a clockwise vortex (viewed from top) and stayed in it driven by a reverse cluster of currents within this zone. The accumulated wood generally entered the zone at the downstream boundary of the vortex. A conceptual model for vortex driven wood rotation was proposed based on the observation to explain the trapping mechanism.
4. The wood length, discharge ratio and release distance had a significant effect on the accumulation probability in the separation zone. Longer wood had a higher probability of being trapped, whereas the accumulation probability gradually dropped or remained nearly constant if the wood length exceeded some critical value. Accumulation probability increased as the discharge ratio increased. The release distance was found to be the most important driver for accumulation. As such distance increased, wood trapping in the separation zone was weaker irrespective of the prevailing conditions.
5. For fully floating wood, the wood did not touch the channel bed. The same pathways under different wood diameter and wood density resulted in negligible effects on the accumulation probability.
6. Based on the observed core factors, three dimensionless controlling parameters were proposed, and a conceptual model for wood accumulation near the confluence was developed for practical application.

This experiment primarily focused on the transport and accumulation of individual wood pieces under sediment-free condition without regard to the effects of the wood geometry (roots or branches). However, congested transport was observed to increase the probability of wood jam formation (Bocchiola et al., 2008), which could have a more significant impact on river morphology and sediment dynamics (Schalko et al., 2019a, 2019b). In future studies, the numerical modeling of wood-flow interaction could be considered to quantify the conceptual model, providing an insightful understanding of the motion of wood near confluences.

Data Availability Statement

Observed data supporting the findings are accessible through ResearchGate (http://dx.doi.org/10.13140/RG.2.2.15404.44167).

Acknowledgments
This research was funded by the National Key R&D Program of China (2022YFC3202602), the National Natural Science Foundation of China (52079044; U2340221), the Natural Science Foundation of Jiangsu Province, China (BK20230036), the Fundamental Research Funds for the Central Universities (B230201057), and the 111 Project (B17015). The authors would like to thank Professor Bidya Sagar Pani of the Indian Institute of Technology-Bombay for help in revising this work. Thanks are also extended to Yunqiang Zhu, Guanghui Yan, Jiawei Lin of Hohai University for their support during the experiment.

References

Abbe, T. B., & Montgomery, D. R. (2003). Patterns and processes of wood debris accumulation in the Queets river basin, Washington. *Geomorphology*, *51*(1–3), 81–107. https://doi.org/10.1016/S0169-555X(02)00326-4

Benda, L., Miller, D. A. N. I. E. L., Sias, J., Martin, D., Bilby, R., Veldhuisen, C., & Dunne, T. (2003). Wood recruitment processes and wood budgeting. In *American fisheries society symposium* (pp. 49–74). American Fisheries Society.

Benda, L., Veldhuisen, C., & Black, J. (2003). Debris flows as agents of morphological heterogeneity at low-order confluences, Olympic Mountains, Washington. *The Geological Society of America Bulletin*, *115*(9), 1110–1121. https://doi.org/10.1130/B25265.1

Benda, L. E. E., Andras, K., Miller, D., & Bigelow, P. (2004). Confluence effects in rivers: Interactions of basin scale, network geometry, and disturbance regimes. *Water Resources Research*, *40*(5). https://doi.org/10.1029/2003WR002583

Best, J. L. (1987). *Flow dynamics at river channel confluences: Implications for sediment transport and bed morphology*. In F. G. Ethridge, R. M. Flores, & M. D. Harvey (Eds.), *Recent developments in fluvial sedimentology* (Vol. 39, pp. 27–35). https://doi.org/10.2110/pec.87.39.0027

Best, J. L. (1988). Sediment transport and bed morphology at river channel confluences. *Sedimentology*, *35*(3), 481–498. https://doi.org/10.1111/j.1365-3091.1988.tb00999.x

Best, J. L., & Reid, I. (1984). Separation zone at open-channel junctions. *Journal of Hydraulic Engineering*, *110*(11), 1588–1594. https://doi.org/10.1061/(ASCE)0733-9429(1984)110:11(1588)

Bocchiola, D., Catalano, F., Menduni, G., & Passoni, G. (2002). An analytical–numerical approach to the hydraulics of floating debris in river Channel_2. *Journal of Hydrology*, *269*(1–2), 65–78. https://doi.org/10.1016/S0022-1694(02)00195-6

Bocchiola, D., Rulli, M. C., & Rosso, R. (2006). Transport of large woody debris in the presence of obstacles. *Geomorphology*, *76*(1–2), 166–178. https://doi.org/10.1016/j.geomorph.2005.08.016

Bocchiola, D., Rulli, M. C., & Rosso, R. (2008). A flume experiment on the formation of wood jams in rivers. *Water Resources Research*, *44*(2). https://doi.org/10.1029/2006WR005846

Braudrick, C. A., & Grant, G. E. (2001). Transport and deposition of large woody debris in streams: A flume experiment. *Geomorphology*, *41*(4), 263–283. https://doi.org/10.1016/S0169-555X(01)00058-7

Braudrick, C. A., Grant, G. E., Ishikawa, Y., & Ikeda, H. (1997). Dynamics of wood transport in streams: A flume experiment. *Earth Surface Processes and Landforms: The Journal of the British Geomorphological Group*, *22*(7), 669–683. https://doi.org/10.1002/(SICI)1096-9837(199707)22:7%3C669::AID-ESP740%3E3.0.CO;2-L

Buxton, T. H. (2010). Modeling entrainment of waterlogged large wood in stream channels. *Water Resources Research*, *46*(10). https://doi.org/10.1029/2009WR008041

Collins, B. D., Montgomery, D. R., & Haas, A. D. (2002). Historical changes in the distribution and functions of large wood in Puget Lowland rivers. *Canadian Journal of Fisheries and Aquatic Sciences*, *59*(1), 66–76. https://doi.org/10.1139/f01-199

Comiti, F., Andreoli, A., Lenzi, M. A., & Mao, L. (2006). Spatial density and characteristics of woody debris in five mountain rivers of the Dolomites (Italian Alps). *Geomorphology*, *78*(1–2), 44–63. https://doi.org/10.1016/j.geomorph.2006.01.021

Comiti, F., Lucía, A., & Rickenmann, D. (2016). Large wood recruitment and transport during large floods: A review. *Geomorphology*, *269*, 23–39. https://doi.org/10.1016/j.geomorph.2016.06.016

Davidson, S. L., MacKenzie, L. G., & Eaton, B. C. (2015). Large wood transport and jam formation in a series of flume experiments. *Water Resources Research*, *51*(12), 10065–10077. https://doi.org/10.1002/2015WR017446

Diehl, T. H. (1997). *Potential drift accumulation at bridges*. US Department of Transportation, Federal Highway Administration, Research and Development, Turner-Fairbank Highway Research Center.

Fausch, K. D. (1993). Experimental analysis of microhabitat selection by juvenile steelhead (Oncorhynchus mykiss) and coho salmon (O. kisutch) in a British Columbia stream. *Canadian Journal of Fisheries and Aquatic Sciences*, *50*(6), 1198–1207. https://doi.org/10.1139/f93-136

Furlan, P., Pfister, M., Matos, J., Amado, C., & Schleiss, A. J. (2019). Experimental repetitions and blockage of large stems at ogee crested spillways with piers. *Journal of Hydraulic Research*, *57*(2), 250–262. https://doi.org/10.1080/00221686.2018.1478897

Furlan, P., Pfister, M., Matos, J., Amado, C., & Schleiss, A. J. (2020). Statistical accuracy for estimations of large wood blockage in a reservoir environment. *Environmental Fluid Mechanics*, *20*(3), 579–592. https://doi.org/10.1007/s10652-019-09708-7

Furlan, P., Pfister, M., Matos, J., Amado, C., & Schleiss, A. J. (2021). Blockage probability modeling of large wood at reservoir spillways with piers. *Water Resources Research*, *57*(8), e2021WR029722. https://doi.org/10.1029/2021WR029722

Gippel, C. J., O'Neill, I. C., Finlayson, B. L., & Schnatz, I. N. G. O. (1996). Hydraulic guidelines for the re-introduction and management of large woody debris in lowland rivers. *Regulated Rivers: Research and Management*, *12*(2-3), 223–236. https://doi.org/10.1002/(SICI)1099-1646(199603)12:2/3%3C223::AID-RRR391%3E3.0.CO;2-%23

Gualtieri, C., Abdi, R., Ianniruberto, M., Filizola, N., & Endreny, T. A. (2020). A 3D analysis of spatial habitat metrics about the confluence of Negro and Solimões rivers, Brazil. *Ecohydrology*, *13*(1), e2166. https://doi.org/10.1002/eco.2166

Gualtieri, C., Ianniruberto, M., & Filizola, N. (2019). On the mixing of rivers with a difference in density: The case of the Negro/Solimões confluence, Brazil. *Journal of Hydrology*, *578*, 124029. https://doi.org/10.1016/j.jhydrol.2019.124029

Gurnell, A., Piégay, H., Swanson, F., & Gregory, S. (2002). Large wood and fluvial processes. *Freshwater Biology*, *47*(4), 601–619. https://doi.org/10.1046/j.1365-2427.2002.00916.x

Gurnell, A., Tockner, K., Edwards, P., & Petts, G. (2005). Effects of deposited wood on biocomplexity of river corridors. *Frontiers in Ecology and the Environment*, *3*(7), 377–382. https://doi.org/10.1890/1540-9295(2005)003[0377:EODWOB]2.0.CO;2

Haga, H., Kumagai, T. O., Otsuki, K., & Ogawa, S. (2002). Transport and retention of coarse woody debris in mountain streams: An in situ field experiment of log transport and a field survey of coarse woody debris distribution. *Water Resources Research*, *38*(8), 1. https://doi.org/10.1029/2001WR001123

Innocenti, L., Branß, T., Zaid, B., Aberle, J., & Solari, L. (2023). Characterization of trajectories and drag coefficients of large wood in sharp river bends from flume experiments. *Earth Surface Processes and Landforms*, *48*(4), 770–781. https://doi.org/10.1002/esp.5516

Johnson, S. L., Rodgers, J. D., Solazzi, M. F., & Nickelson, T. E. (2005). Effects of an increase in large wood on abundance and survival of juvenile salmonids (Oncorhynchus spp.) in an Oregon coastal stream. *Canadian Journal of Fisheries and Aquatic Sciences*, *62*(2), 412–424. https://doi.org/10.1139/f04-222

Keller, E. A., & Swanson, F. J. (1979). Effects of large organic material on channel form and fluvial processes. *Earth Surface Processes*, *4*(4), 361–380. https://doi.org/10.1002/esp.3290040406

Lancaster, S. T., Hayes, S. K., & Grant, G. E. (2003). Effects of wood on debris flow runout in small mountain watersheds. *Water Resources Research*, *39*(6). https://doi.org/10.1029/2001WR001227

Lucía, A., Comiti, F., Borga, M., Cavalli, M., & Marchi, L. (2015). Dynamics of large wood during a flash flood in two mountain catchments. *Natural Hazards and Earth System Sciences*, *15*(8), 1741–1755. https://doi.org/10.5194/nhess-15-1741-2015

Lyn, D. A., Cooper, T. J., Yi, Y. K., Sinha, R. N., & Rao, A. R. (2003). Debris accumulation at bridge crossings: Laboratory and field studies. https://doi.org/10.5703/1288284313171

Manners, R. B., Doyle, M., & Small, M. J. (2007). Structure and hydraulics of natural woody debris jams. *Water Resources Research*, *43*(6). https://doi.org/10.1029/2006WR004910

Marcus, W. A., Marston, R. A., Colvard, C. R., Jr., & Gray, R. D. (2002). Mapping the spatial and temporal distributions of woody debris in streams of the Greater Yellowstone Ecosystem, USA. *Geomorphology*, *44*(3–4), 323–335. https://doi.org/10.1016/S0169-555X(01)00181-7

Moulin, B., & Piégay, H. (2004). Characteristics and temporal variability of large woody debris trapped in a reservoir on the River Rhone: Implications for river basin management. *River Research and Applications*, *20*(1), 79–97. https://doi.org/10.1002/rra.724

Nagayama, S., Nakamura, F., Kawaguchi, Y., & Nakano, D. (2012). Effects of configuration of instream wood on autumn and winter habitat use by fish in a large remeandering reach. *Hydrobiologia*, *680*(1), 159–170. https://doi.org/10.1007/s10750-011-0913-z

Nokes, R. (2017). *Streams v2.06: System theory and design*. University of Canterbury.

Panici, D. (2021). An experimental and numerical approach to modeling large wood displacement in rivers. *Water Resources Research*, *57*(7), e2021WR029860. https://doi.org/10.1029/2021WR029860

Persi, E., Petaccia, G., & Sibilla, S. (2018). Large wood transport modelling by a coupled Eulerian–Lagrangian approach. *Natural Hazards*, *91*, 59–74. https://doi.org/10.1007/s11069-017-2891-6

Persi, E., Petaccia, G., Sibilla, S., Brufau, P., & García-Navarro, P. (2019). Calibration of a dynamic Eulerian-Lagrangian model for the computation of wood cylinders transport in shallow water flow. *Journal of Hydroinformatics*, *21*(1), 164–179. https://doi.org/10.2166/hydro.2018.085

Ravazzolo, D., Spreitzer, G., Tunnicliffe, J., & Friedrich, H. (2022). The effect of large wood accumulations with rootwads on local geomorphic changes. *Water Resources Research*, *58*(5), e2021WR031403. https://doi.org/10.1029/2021WR031403

Rhoads, B. L. (2020). *River dynamics: Geomorphology to support management*. Cambridge University Press.

Rhoads, B. L., & Sukhodolov, A. N. (2001). Field investigation of three-dimensional flow structure at stream confluences: 1. Thermal mixing and time-averaged velocities. *Water Resources Research*, *37*(9), 2393–2410. https://doi.org/10.1029/2001WR000316

Rhoads, B. L., & Sukhodolov, A. N. (2004). Spatial and temporal structure of shear-layer turbulence at a stream confluence. *Water Resources Research*, *6*, 2393–2410. https://doi.org/10.1029/2003WR002811

Rhoads, B. L., & Sukhodolov, A. N. (2008). Lateral momentum flux and the spatial evolution of flow within a confluence mixing interface. *Water Resources Research*, *44*(8), 27–143. https://doi.org/10.1029/2007WR006634

Ruiz-Villanueva, V., Bodoque, J. M., Díez-Herrero, A., & Bladé, E. (2014). Large wood transport as significant influence on flood risk in a mountain village. *Natural Hazards*, *74*(2), 967–987. https://doi.org/10.1007/s11069-014-1222-4

Ruiz-Villanueva, V., Piégay, H., Gaertner, V., Perret, F., & Stoffel, M. (2016). Wood density and moisture sorption and its influence on large wood mobility in rivers. *Catena*, *140*, 182–194. https://doi.org/10.1016/j.catena.2016.02.001

Ruiz-Villanueva, V., Wyżga, B., Zawiejska, J., Hajdukiewicz, M., & Stoffel, M. (2016). Factors controlling large-wood transport in a mountain river. *Geomorphology*, *272*, 21–31. https://doi.org/10.1016/j.geomorph.2015.04.004

Schalko, I., Lageder, C., Schmocker, L., Weitbrecht, V., & Boes, R. M. (2019a). Laboratory flume experiments on the formation of spanwise large wood accumulations: I. Effect on backwater rise. *Water Resources Research*, *55*(6), 4854–4870. https://doi.org/10.1029/2019WR024789

Schalko, I., Lageder, C., Schmocker, L., Weitbrecht, V., & Boes, R. M. (2019b). Laboratory flume experiments on the formation of spanwise large wood accumulations: Part II—Effect on local scour. *Water Resources Research*, *55*(6), 4871–4885. https://doi.org/10.1029/2018WR024649

Schalko, I., Schmocker, L., Weitbrecht, V., & Boes, R. M. (2018). Backwater rise due to large wood accumulations. *Journal of Hydraulic Engineering*, *144*(9), 04018056. https://doi.org/10.1061/(ASCE)HY.1943-7900.0001501

Schalko, I., Schmocker, L., Weitbrecht, V., & Boes, R. M. (2020). Laboratory study on wood accumulation probability at bridge piers. *Journal of Hydraulic Research*, *58*(4), 566–581. https://doi.org/10.1080/00221686.2019.1625820

Schmocker, L., & Hager, W. H. (2011). Probability of drift blockage at bridge decks. *Journal of Hydraulic Engineering*, *137*(4), 470–479. https://doi.org/10.1061/(ASCE)HY.1943-7900.0000319

Spreitzer, G., Tunnicliffe, J., & Friedrich, H. (2021). Effects of large wood (LW) blockage on bedload connectivity in the presence of a hydraulic structure. *Ecological Engineering*, *161*, 106156. https://doi.org/10.1016/j.ecoleng.2021.106156

Tang, H., Yuan, S., & Cao, H. (2023). Theory and practice of hydrodynamic reconstruction in plain river networks. *Engineering*, *24*, 202–211. https://doi.org/10.1016/j.eng.2022.01.015

Van den Bremer, T., Whittaker, C., Calvert, R., Raby, A., & Taylor, P. (2019). Experimental study of particle trajectories below deep-water surface gravity wave groups. *Journal of Fluid Mechanics*, *879*, 168–186. https://doi.org/10.1017/jfm.2019.584

Welber, M., Bertoldi, W., & Tubino, M. (2013). Wood dispersal in braided streams: Results from physical modeling. *Water Resources Research*, *49*(11), 7388–7400. https://doi.org/10.1002/2013WR014046

Whittaker, C., Nokes, R., & Davidson, M. (2015). Tsunami forcing by a low Froude number landslide. *Environmental Fluid Mechanics*, *15*(6), 1215–1239. https://doi.org/10.1007/s10652-015-9411-6

Wohl, E. (2017). Bridging the gaps: An overview of wood across time and space in diverse rivers. *Geomorphology*, *279*, 3–26. https://doi.org/10.1016/j.geomorph.2016.04.014

Wohl, E., Bledsoe, B. P., Fausch, K. D., Kramer, N., Bestgen, K. R., & Gooseff, M. N. (2016). Management of large wood in streams: An overview and proposed framework for hazard evaluation. *JAWRA Journal of the American Water Resources Association*, *52*(2), 315–335. https://doi.org/10.1111/1752-1688.12388

Wohl, E., Cenderelli, D. A., Dwire, K. A., Ryan-Burkett, S. E., Young, M. K., & Fausch, K. D. (2010). Large in-stream wood studies: A call for common metrics. *Earth Surface Processes and Landforms: The Journal of the British Geomorphological Research Group*, *35*(5), 618–625. https://doi.org/10.1002/esp.1966

Xu, L., Yuan, S., Tang, H., Qiu, J., Xiao, Y., Whittaker, C., & Gualtieri, C. (2022). Mixing dynamics at the large confluence between the Yangtze River and Poyang lake. *Water Resources Research*, *58*(11), e2022WR032195. https://doi.org/10.1029/2022WR032195

Yuan, S., Qiu, J., Tang, H., Xu, L., Xiao, Y., Liu, M., et al. (2023). Fish community traits near a large confluence: Implications for its nodal effects in the river ecosystem. *Journal of Hydrology*, *626*, 130335. https://doi.org/10.1016/j.jhydrol.2023.130335

Yuan, S., Tang, H., Li, K., Xu, L., Xiao, Y., Gualtieri, C., et al. (2021). Hydrodynamics, sediment transport and morphological features at the confluence between the Yangtze River and the Poyang Lake. *Water Resources Research*, *57*(3), e2020WR028284. https://doi.org/10.1029/2020WR028284

Yuan, S., Tang, H., Xiao, Y., Qiu, X., & Xia, Y. (2018). Water flow and sediment transport at open-channel confluences: An experimental study. *Journal of Hydraulic Research*, *56*(3), 333–350. https://doi.org/10.1080/00221686.2017.1354932

Yuan, S., Tang, H., Xiao, Y., Qiu, X., Zhang, H., & Yu, D. (2016). Turbulent flow structure at a 90-degree open channel confluence: Accounting for the distortion of the shear layer. *Journal of Hydro-environment Research*, *12*, 130–147. https://doi.org/10.1016/j.jher.2016.05.006

Yuan, S., Tang, H., Xiao, Y., Xia, Y., Melching, C., & Li, Z. (2019). Phosphorus contamination of the surface sediment at a river confluence. *Journal of Hydrology*, *573*, 568–580. https://doi.org/10.1016/j.jhydrol.2019.02.036

Yuan, S., Xu, L., Tang, H., Xiao, Y., & Gualtieri, C. (2022). The dynamics of river confluences and their effects on the ecology of aquatic environment: A review. *Journal of Hydrodynamics*, *34*(1), 1–14. https://doi.org/10.1007/s42241-022-0001-z

Yuan, S., Yan, G., Tang, H., Xiao, Y., Rahimi, H., Aye, M. N., & Gualtieri, C. (2023). Effects of tributary floodplain on confluence hydrodynamics. *Journal of Hydraulic Research*, *61*(4), 552–572. https://doi.org/10.1080/00221686.2023.2231413

Yuan, S., Zhu, Y., Tang, H., Xu, L., Li, K., Xiao, Y., & Gualtieri, C. (2022). Planform evolution and hydrodynamics near the multi-channel confluence between the Yarlung Zangbo River and the delta of the Niyang River. *Geomorphology*, *402*, 108157. https://doi.org/10.1016/j.geomorph.2022.108157